HHS Public Access

Author manuscript

J Magn Reson Imaging. Author manuscript; available in PMC 2018 March 01.

Published in final edited form as:

J Magn Reson Imaging. 2017 March ; 45(3): 872–878. doi:10.1002/jmri.25398.

7T MRI of Distal Radius Trabecular Bone Microarchitecture: How Trabecular Bone Quality Varies Depending on Distance from End-of-Bone

Lindsay M Griffin, MD[1], **Stephen Honig, MD**[2], **Cheng Chen, M.S.**[3], **Punam K Saha, PhD**[3], **Ravinder Regatte, PhD**[1], and **Gregory Chang, MD**[1]

[1]Department of Radiology, New York University School of Medicine, New York, NY

[2]Department of Medicine, New York University School of Medicine, New York, NY

[3]Departments of Radiology and Electrical and Computer Engineering, University of Iowa, Iowa City, IA

Abstract

Purpose—To use 7 T magnetic resonance imaging (MRI) to determine how trabecular bone microarchitecture varies at the epiphysis, metaphysis, and diaphysis of the distal radius.

Materials and Methods—The distal radius of 24 females (mean age = 56 years, range = 24–78 years) was scanned on a 7T MRI using a 3-D fast low-angle shot sequence (0.169 mm × 0.169 mm × 1 mm). Digital topological analysis was applied at the epiphysis, metaphysis, and diaphysis to compute: total trabecular bone volume; trabecular thickness, number, connectivity, and erosion index (a measure of network resorption). Differences and correlations were assessed using standard statistical methods.

Results—The metaphysis and epiphysis had 83–123% greater total bone volume and 14–16% greater trabecular number than the diaphysis (both $p < .0001$). The erosion index was significantly higher at the diaphysis than the metaphysis and epiphysis (both $p < .01$). The most elderly volunteers had lower trabecular number (< 66 years mean 0.29±0.01; ≥ 66 years, 0.27±0.02, $p < .05$) and higher erosion index (< 66 years mean 1.18±0.17; age ≥ 66 years, mean 1.42±0.46, $p < .05$) at the epiphysis; differences not detected by total trabecular bone volume.

Conclusion—7T MRI reveals trabecular bone microarchitecture varies depending on scan location at the end-of-bone, being of overall higher quality distally (epiphysis) than proximally (diaphysis). Age-related differences in trabecular microarchitecture can be detected by 7T MRI. The results highlight the potential sensitivity of 7T MRI to microarcitectural differences and the potential importance of standardizing scan location for future clinical studies of fracture risk or treatment response.

Corresponding author: Lindsay Griffin, Bellevue Hospital Center/NYU School of Medicine, Department of Radiology 3W-37, 462 First Avenue, New York, New York 10016, Lindsay.Griffin@nyumc.org, 608-698-5551.

Disclosure Statement: G.C. was paid a consulting fee from Siemens for an educational lecture unrelated to this research.

Key Terms

7T MRI; Radius; Trabecular bone; Microarchitecture

INTRODUCTION

Osteoporosis is a disease of increased fracture risk due to low bone mass and microarchitectural deterioration of bone tissue (1). Osteoporosis is a common disease, affecting one in two women and one in five men over fifty years old (2). Prior estimates have shown that 10 million Americans over age 50 have osteoporosis at the hip and 33.6 million have osteopenia at the hip (3). Moreover, osteoporotic fractures, especially of the hip and spine, have considerable associated mortality and morbidity (4 – 6). Hence, diagnosis and treatment of osteoporosis prior to fracture is crucial.

Bone strength is determined by both bone mass and microarchitecture (7). Imaging is an important component in assessment of fracture risk (8). Dual-energy x-ray absorptiometry (DXA) estimation of areal bone mineral density (BMD) is the standard-of-care test used to diagnose osteoporosis and provides a metric of bone mass. However, DXA has limitations. First, BMD accounts for only approximately 60% of bone strength (9). Second, DXA is a two-dimensional imaging method and is vulnerable to over- or under-estimation based on bone size (10). Finally, DXA does not account for bone microarchitecture, which also plays a critical role in bone strength. In the last 15 years, imaging of bone microarchitecture has become possible via micro-magnetic resonance imaging (MRI) methods (11 – 13) and high-resolution peripheral quantitative computed tomography (HR-pQCT) (14, 15). Imaging of bone microarchitecture is important because there is evidence it provides useful information about fracture risk and mechanisms of action of osteoporosis therapies that cannot be provided by DXA (9, 16).

Our purpose is to determine how trabecular bone microarchitectural parameters and their interrelationships vary at the epiphysis, metaphysis, and diaphysis of the distal radius, intrinsically and in relation to age and fracture status.

MATERIALS AND METHODS

Study Population

This study was approved by our Institutional Review Board and written informed consent was obtained from all participants. Twenty four healthy female volunteers without history of trauma, surgery, arthropathy, or metabolic/endocrine disorder were recruited. We studied only female subjects in this initial study in order to eliminate the possible confounding variable of gender, as male-female differences in bone microarchitecture could exist.

MRI Acquisition

Subjects were scanned on a 7T whole body MR scanner (Siemens, Erlangen, Germany) in the prone position with the non-dominant wrist extended in front of them (“superman” position). An 8-channel receive coil, constructed in-house and consisting of two curved

"clamshell" sections, was used (17). The technical specifications of this coil (which was specifically designed for use at 7T), including signal-to-noise ratio (SNR) maps, B1+ maps, and parallel imaging performance were previously published (17). Axial images of the distal radius were obtained with a 3-dimensional fast low-angle shot sequence (3-D FLASH, TR/TE = 20 msec/4.1 msec, flip angle = 10°, field-of-view = 86 mm, matrix = 512 × 512, resolution = 0.169 mm × 0.169 mm, 40 axial images, slice thickness = 1 mm, parallel imaging (GRAPPA) acceleration factor = 2, imaging time = 4 minutes 6 seconds) as previously described (17, 18). No subjects reported claustrophobia nor other adverse events.

Image Analysis

We analyzed bone microarchitecture within 10 mm-thick volumes of interest in three locations: the distal radial epiphysis, metaphysis and diaphysis. The epiphysis was defined as the ten most distal axial slices within the distal radius. The metaphyseal volume of interest was defined as the ten axial slices just proximal to the epiphyseal volume of interest, and the diaphyseal volume of interest was defined as the ten axial slices just proximal to the metaphyseal volume of interest. To each volume of interest, we applied digital topological analysis (DTA) (19, 20). DTA is a 3-D method that accurately determines the topological class (e.g., surfaces, curves, junctions) of each individual location in a digitized structure that has been applied for quantifying quality of trabecular bone architectural makeup. Before applying DTA, a binarized trabecular bone image is skeletonized to a network of 1-D and 2-D structures representing rods and plates, respectively. DTA involves inspecting each bone voxel's neighboring voxels (i.e., the 26 other voxels within the voxel's 3 × 3 × 3 kernel) and subsequent computation of trabecular parameters. A unique topological classification can be achieved using lookup tables solving for local topological ambiguities in digital manifolds and their junctions. These topological classes are then used to compute several topological parameters for trabecular bone networks.

We computed: total trabecular bone volume, apparent trabecular thickness, and markers of trabecular number, trabecular network connectivity (junc, a measure of connections between trabecular rods and plates), and erosion index (a measure of trabecular network resorption secondary to osteoclasts). More specifically, total bone volume refers only to the total volume occupied by individual trabecular bone structures inside the trabecular compartment, which was separated from cortical bone via manual outlining under the guidance of a musculoskeletal radiologist. Note that the other term "total volume" represents the volume of outlined trabecular compartment including individual trabecular bone structures as well as the marrow space. Junc is a marker of trabecular microarchitecture, which refers to the normalized count of voxels forming topological junctions of individual trabeculae inside the trabecular compartment. Erosion index was defined as the ratio of all topological parameters expected to increase with trabecular bone erosion (e.g., rods, plate-edges, and rod junctions) to all those that are expected to decrease by erosion (e.g., plate interiors and plate junctions)." Previous bone biopsy studies of patients with osteoporosis have shown alterations in these parameters compared to controls (21, 22).

The coefficient of variation for microarchitectural parameters at 7T with this image analysis and MRI technique has previously been shown to be 0.8–5.6 % (18, 23). Each scan was

evaluated on a 5 point scale for image quality (1 = non-visualization, 2 = poor, 3 = good, 4, = very good, 5 = excellent) by one of the authors, a musculoskeletal radiologist. On this scale, 5 represented the highest quality and denoting ability to clearly visualize sharp and distinct trabeculae and 1 represented the lowest quality denoting the inability to visualize any trabeculae. The mean image quality score was 4.3±0.7 with all images scoring ≥3, No images were excluded in final analyses. Figure 1 is an example of images used for analysis at each site and Figure 2 is an example of how DTA was performed.

Statistical Analysis

Analyses were performed using Stata 13.0 (StataCorp). $P < .05$ was considered significant and two-sided tests were used through-out. Differences between bone sites were assessed using paired Student t-tests or Wilcoxon signed-rank test when data was non-normally distributed. Correlations between parameters at each site were assessed by Spearman rank correlation. Spearman correlation was used because it allows for assessment of correlation between non-parametric, monotonic (but not necessarily linear) data. In order to account for differences in total bone volume (because of differences in total bone volume at each site), multivariate linear regression was used to assess between-site-differences in trabecular architecture for a given total bone volume, with the exception of trabecular number which was not significantly associated with total bone volume. We also adjusted for total bone volume by using 1/(total bone volume) as a weighting factor in the analysis, giving more weight to measures with higher or lower total bone volume depending on whether the correlation of the measure with total bone volume is negative or positive, respectively. Age effects were assessed using age quartiles. Subgroup comparisons for subjects with versus without fracture were performed using Student's t-tests and multivariate regression. The assumptions for regression models were assessed using quantile-quantile plots to assess the normality of residuals.

RESULTS

The mean age of the twenty four healthy female volunteers was 55±14 years (quartile age ranges were 24–51 years, 52–60 years, 61–65 years, and 66–78 years.) Fourteen volunteers reported history of fracture. Median number of fractures was 3 (rage 1–5) amongst those who reported fracture.

Overall trabecular bone quality increased from the diaphysis towards the epiphysis with higher total trabecular bone volume, trabecular number, and trabecular connectivity, and lower erosion index at the metaphysis/epiphysis in comparison with the diaphysis. As demonstrated in the MRI images in Figure 1 and in the values in Table 1, the most striking increase was in total trabecular bone volume. Total trabecular bone volume was, on average, 123% higher at the metaphysis and 306% higher at the epiphysis than at the diaphysis. Trabecular number was, on average, 12% higher at the metaphysis and 16% higher at the epiphysis than at the diaphysis. Trabecular thickness was not significantly different between sites. Trabecular connectivity was on average 25% higher at the metaphysis and 50% higher at the epiphysis than at the diaphysis. Lastly, the erosion index was 24% lower at the metaphysis and 17% lower at the epiphysis than at the diaphysis, on average. Figure 2 shows

differences between a subject with relatively high trabecular bone volume and a subject with relatively low trabecular bone volume.

Correlations of bone parameters including p values are shown in Table 2. Of note, total trabecular bone volume, erosion index, and trabecular thickness were significantly correlated at all sites. Trabecular number was strongly correlated with connectivity. Trabecular number did not correlate with total trabecular bone volume nor trabecular thickness at any site. Erosion index correlated with trabecular number at the metaphysis and with connectivity at the diaphysis.

Because of the large differences in total trabecular bone volume between sites, we assessed whether differences in the other trabecular bone microarchitectural parameters between sites were affected by total trabecular bone volume and how parameters changed after adjusting for total trabecular bone volume. Total trabecular bone volume was not significant in the models of trabecular number. After adjusting for total trabecular bone volume, trabecular thickness was significantly less at the metaphysis and epiphysis in comparison with the diaphysis (all $p < 0.0001$). Trabecular connectivity was higher at the metaphysis than the diaphysis and epiphysis (both $p < 0.05$) and the epiphysis had a higher erosion index than the diaphysis and metaphysis (both $p < 0.0001$). Overall, total trabecular bone volume drives the absolute differences in trabecular thickness, connectivity, and erosion index between sites.

Differences in bone parameters related to age and fracture status were also assessed. Trabecular number at the epiphysis was significantly lower in the oldest quartile of volunteers (age ≥ 66) in comparison with the other quartiles (age < 66 years, mean trabecular number 0.29±0.01 versus age ≥ 66 years, mean trabecular number 0.27±0.02, $p < .05$). Erosion index at the epiphysis was significantly higher in the eldest quartile of volunteers (age < 66 years, mean erosion index 1.18±0.17 versus age ≥ 66 years, mean erosion index 1.42±0.46, $p < .05$). These effects persisted after controlling for total trabecular bone volume in multivariate regression analysis. Age-related differences were not observed at the metaphysis nor diaphysis. Differences in bone parameters at the three sites were not detected between those with or without fracture.

DISCUSSION

Osteoporosis is a disease of weak bone and increased fracture risk secondary to low bone mass and microarchitectural deterioration of bone tissue (1). DXA provides clinicians with a means to assess bone mass. With the recent arrival of novel imaging technologies, such as HR-pQCT and micro-MRI, clinicians and researchers now have the ability to image and monitor changes in bone microarchitecture in vivo.

Although osteoporosis is a systemic disease affecting all bones in the skeleton, we hypothesized that variation in bone microarchitecture exists along the longitudinal axis of bone. Prior studies in cadaveric human specimens (24) and in humans in vivo using MRI (25) have shown that percent trabecular bone, total bone mass, and trabecular bone volume fraction decrease and trabecular separation increases as the distance from the end of bone

increases. In this study, we used 7T MRI to build on these prior studies and define the microarchitectural basis for the changes in bone mass and quality along the longitudinal axis of the distal radius. Our results show that trabecular bone microarchitecture does change depending on whether it is assessed in the epiphysis, metaphysis, or distal diaphysis and was of overall higher quality at the epiphysis and metaphysis compared to the diaphysis.

We found that the differences in trabecular bone microarchitectural parameters at the epiphysis and metaphysis relative to the diaphysis were mediated by increases in total trabecular bone volume. The question as to why the body would need to increase trabecular bone microarchitectural quality and total trabecular bone volume (a marker of bone mass) at the end-of-bone is an interesting one. Though the focus of this study was on trabecular bone microarchitecture, we conjecture that the improvements in trabecular bone microarchitecture and increase in total bone volume in the epiphysis/metaphysis compared to the diaphysis may reflect the body's need for higher trabecular bone quality in locations where cortical bone is very thin, such as at the end of bone. In vertebral bodies, where the cortex is also very thin, biomechanical and finite element analysis studies have shown that it is trabecular bone microarchitecture, rather than cortical bone, that is critical the contributor to bone strength (26). Future work in the distal radius could be directed at quantifying both cortical and trabecular bone parameters in similar studies using finite element modeling in order to assess the contributions of cortical and trabecular bone to overall bone strength at different distal radius locations.

We found decreased bone quality at the epiphysis in terms of trabecular number and erosion index in the eldest of our population in comparison with the rest. There is a 30-fold rise in fracture risk between the ages of 50 and 80 that is not explained by BMD (27). Since bone microarchitecture is an important contributor to bone strength independent of BMD, it may be possible that deteriorated microarchitecture may explain elevated fracture risk in elderly subjects, in particular at skeletal sites where trabecular bone contributes the most to bone strength. In the future, it will be important to determine the relationship between microarchitectural deterioration and fracture risk in longitudinal studies.

The finding that trabecular bone microarchitectural quality was overall higher at the epiphysis and metaphysis than at the diaphysis may at first seem surprising given that distal radius fractures, such as the Colles fracture, typically occur within 1 cm of the articular surface, in the epiphysis or metaphysis, rather than at the diaphysis (28). However, this seemingly surprising result, can perhaps be explained by Wolff's Law and the pathomechanics of distal radius fractures. Wolff's Law states bone remodels in response to the mechanical loads placed upon it (29). Because a distal radius fracture is usually caused by a fall on an outstretched hand, abnormal axial forces are exerted first on the epiphysis and then on the underlying metaphysis at the time of the fall (30). Since the distal radial epiphysis and metaphysis are not habituated to such high axial mechanical loads, then the trabecular microarchitectural network in the epiphysis and metaphysis will not be organized in a manner to withstand these forces, and a fracture will result. This will be particularly true in an osteoporotic patient in whom microarchitectural deterioration exists. Because the mechanical energy of the axial load will be dissipated in fracturing the epiphysis and

metaphysis, the distal diaphysis, being deepest in distance from the site of the axial load, will be the less likely location to fracture in the setting of a fall on an outstretched hand.

The results of this study also highlight the importance of standardizing scan locations for cross-sectional and longitudinal imaging studies of bone microarchitecture, whether they be performed via micro-MRI or HR-pQCT. If scan locations differ between patients, then it is possible that differences between groups or longitudinal changes over time are simply secondary to systematic differences in scan locations. We believe that the use of anatomic landmarks to define scan location could help alleviate this problem with the understanding dimensions of bone have individual differences which cannot be completely standardized with the use of an anatomic landmark Therefore, in cross-sectional studies between individuals or groups, this will be important to keep in mind as a limitation. However, it may be important for MRI technologists, when acquiring images in a follow-up longitudinal study, to verify the scan is being performed in the same location as in prior scans by looking at the scout localizer images from the prior scans to ensure consistency within individuals. At our institution, the MRI technologists have PACS access on the computer next to the MRI scanner console, which facilitates such comparison. While image registration software could help a researcher or clinician verify that measurement/image analysis is being done in a similar location, it will not be able to correct for a scan performed in a different location, even if the locations differ by less than 10 mm.

Although we could have performed this study at clinical field strength (1.5 or 3T), we decided to perform this study at 7T. Scanning at 7T has technical challenges including increased energy deposition, changes in relaxation times, greater susceptibility artifacts, B1+ field inhomogeneity, and fewer commercially available radiofrequency coils. But one advantage of scanning at 7T is the higher signal-to-noise ratio (SNR), which scales approximately linearly with the strength of the main magnetic field. We were able to use the increased SNR of 7T to achieve a resolution high enough to visualize trabeculae and also implement parallel imaging to decrease scan time; the scanning session was complete in less than 5 minutes (30 seconds for localizers images, 4 minutes 6 seconds for microarchitecture scanning). Because no dedicated wrist coils exist for human 7T MRI scanners, we used an 8-element receive coil that was constructed in-house. As 7T scanners become more widely available, then coil vendors may in parallel increase the number and types of extremity coils that are available for purchase. Finally, none of the subjects in this study reported any adverse effects from being scanned prone and head first in the superman position at 7T; however, we do note that none of the subjects had claustrophobia. For clinical studies in the future, the ability to have an MRI scan time as short as 4 minutes 6 seconds would be useful for patients who have claustrophobia or anxiety about MRI scanning. We believe that even shorter scanning sessions will be possible in the future, possibly through the implementation of higher parallel acceleration factors or pulse sequences that have higher SNR efficiency. It is important to note that this study was not designed to compare 7T with 3T/1.5T. In the future, it will be important to make such a comparison to determine if there is an overall benefit of 7T beyond 3T/1.5T, if any.

This study has limitations. First, the sample size (n = 24) is relatively small and limited to women However, we still had enough power to detect significant differences between

locations as well as age-related differences. With a greater number of subjects, we could detect more subtle differences between locations and in relation to demographics or fracture for other microarchitectural parameters. Second, we recognize 7T MRI scanners are currently not widely available. In addition, MRI of bone microarchitecture was originally performed on 1.5T and 3T scanners, and the knowledge gained from this 7T study can still be applied to studies performed at other field strengths (10 – 13). Third, we did not implement motion correction methods, which have been previously described by Wehrli et al. (31). However, the presence of motion artifacts on the images should only make it more difficult to detect trends. In the future, to the application of motion correction methods will allow us to confirm our results and should make it possible for micro-MRI methods to detect even subtler changes related to aging, between groups, or longitudinally. Finally, we note that the resolution of micro-MRI is not as high as that of HR-pQCT (81 micron isotropic). Nevertheless, we were still able to determine that microarchitectural parameters vary depending on scan location, and the results can still apply to any future HR-pQCT studies. We note that MRI has its advantages compared to HR-pQCT, including the ability to scan different locations along bone's longitudinal axis and also the lack of ionizing radiation.

In conclusion, we have used 7T MRI to demonstrate that trabecular bone microarchitecture varies greatly depending on scan location at the distal radius. We also show the ability of 7T MRI to detect differences in trabecular microarchitecture between age quartiles.. The results provide some insight into the regional variation in trabecular bone microarchitectural quality that exists even within a short segment of bone in healthy subjects. The results also highlight the importance of standardizing scan locations for future cross-sectional and longitudinal imaging studies of bone microarchitecture. This will allow the results to be accurately interpreted and correlated with important clinical outcomes such as fracture status and response to therapy.

Acknowledgments

Funding support: This work was supported by National Institutes of Health Grants K23-AR059748 (to G.C) and RO1-AR066008 (to G.C.).

References

1. Kanis JA. Diagnosis of osteoporosis and assessment of fracture risk. Lancet. 2002; 359:1929–36. [PubMed: 12057569]
2. van Staa TP, Dennison EM, Leufkens HG, Cooper C. Epidemiology of fractures in England and Wales. Bone. 2001; 29:517–22. [PubMed: 11728921]
3. Bone Health and Osteoporosis: A report of the surgeon general. Office of the Surgeon General; 2004.
4. NIH Consensus Development Panel. Osteoporosis prevention, diagnosis, and therapy. JAMA. 2001; 285:785–95. [PubMed: 11176917]
5. Cummings SR, Melton LJ. Epidemiology and outcomes of osteoporotic fractures. Lancet. 2002; 359:1761–7. [PubMed: 12049882]
6. Compston J. Osteoporosis: social and economic impact. Radiol Clin North Am. 2010; 48:477–82. [PubMed: 20609886]
7. Turner CH. Bone strength: current concepts. Ann N Y Acad Sci. 2006; 1068:429–46. [PubMed: 16831941]

8. Schneider R. Imaging of osteoporosis. Rheum Dis Clin North Am. 2013; 39:609–31. [PubMed: 23719078]
9. Wehrli FW. Structural and functional assessment of trabecular and cortical bone by micro magnetic resonance imaging. J Magn Reson Imaging. 2007; 25:390–409. [PubMed: 17260403]
10. Prentice A, Parsons TJ, Cole TJ. Uncritical use of bone mineral density in absorptiometry may lead to size-related artifacts in the identification of bone mineral determinants. Am J Clin Nutr. 1994; 60:837–42. [PubMed: 7985621]
11. Majumdar S, Link TM, Augat P, et al. Trabecular bone architecture in the distal radius using magnetic resonance imaging in subjects with fractures of the proximal femur. Magnetic Resonance Science Center and Osteoporosis and Arthritis Research Group. Osteoporos Int. 1999; 10:231–9. [PubMed: 10525716]
12. Link TM, Lotter A, Beyer F, et al. Changes in calcaneal trabecular bone structure after heart transplantation: an MR imaging study. Radiology. 2000; 217:855–62. [PubMed: 11110954]
13. Wehrli FW, Hwang SN, Ma J, Song HK, Ford JC, Haddad JG. Cancellous bone volume and structure in the forearm: noninvasive assessment with MR microimaging and image processing. Radiology. 1998; 206:347–57. [PubMed: 9457185]
14. Boutroy S, Bouxsein ML, Munoz F, Delmas PD. In vivo assessment of trabecular bone microarchitecture by high-resolution peripheral quantitative computed tomography. J Clin Endocrinol Metab. 2005; 90:6508–15. [PubMed: 16189253]
15. Cheung AM, Adachi JD, Hanley DA, et al. High-resolution peripheral quantitative computed tomography for the assessment of bone strength and structure: a review by the Canadian Bone Strength Working Group. Curr Osteoporos Rep. 2013; 11:136–46. [PubMed: 23525967]
16. Wehrli FW, Ladinsky GA, Jones C, et al. In vivo magnetic resonance detects rapid remodeling changes in the topology of the trabecular bone network after menopause and the protective effect of estradiol. J Bone Miner Res. 2008; 23:730–40. [PubMed: 18251704]
17. Chang G, Friedrich KM, Wang L, et al. MRI of the wrist at 7 tesla using an eight-channel array coil combined with parallel imaging: preliminary results. J Magn Reson Imaging. 2010; 31:740–6. [PubMed: 20187221]
18. Chang G, Wang L, Liang G, et al. Quantitative assessment of trabecular bone microarchitecture of the wrist via 7 Tesla MRI: preliminary results. MAGMA. 2011; 24:191–9. [PubMed: 21544680]
19. Saha PK, Chaudhuri BB. 3D digital topology under binary transformation with applications. Comput Vis Image Underst. 1996; 63:418–429.
20. Saha PK, Gomberg BR, Wehrli FW. Three-dimensional digital topological characterization of cancellous bone architecture. Int J Imaging Syst Technol. 2000; 11:81–90.
21. Kleerekoper M, Villanueva AR, Stanciu J, Rao DS, Parfitt AM. The role of three-dimensional trabecular microstructure in the pathogenesis of vertebral compression fractures. Calcif Tissue Int. 1985; 37:594–597. [PubMed: 3937580]
22. Amling M, Posl M, Ritzel H, et al. Architecture and distribution of cancellous bone yield vertebral fracture clues. A histomorphometric analysis of the complete spinal column from 40 autopsy specimens. Arch Orthop Trauma Surg. 1996; 115:262–269. [PubMed: 8836458]
23. Chang G, Wang L, Liang G, Babb JS, Saha PK, Regatte RR. Reproducibility of subregional trabecular bone micro-architectural measures derived from 7-Tesla magnetic resonance images. MAGMA. 2011; 24:121–125. [PubMed: 21221706]
24. Schlenker RA, VonSeggen WW. The distribution of cortical and trabecular bone mass along the lengths of the radius and ulna and the implications for in vivo bone mass measurements. Calcif Tissue Res. 1976; 20:41–52. [PubMed: 1260492]
25. Majumdar S, Genant HK, Grampp S, et al. Correlation of trabecular bone structure with age, bone mineral density, and osteoporotic status: in vivo studies in the distal radius using high resolution magnetic resonance imaging. J Bone Miner Res. 1997; 12:111–118. [PubMed: 9240733]
26. Fields AJ, Ewaran SK, Jekir MG, Keaveney TM. Role of trabecular microarchitecture in whole-vertebral body biomechanical behavior. J Bone Miner Res. 2009; 24:1523–1530. [PubMed: 19338454]
27. Kanis JA, Borgstrom F, De Laet C, et al. Assessment of fracture risk. Osteoporos Int. 2005; 16:581–589. [PubMed: 15616758]

28. Distal Radius Fractures (Broken Wrist). [10/8/2015] Orthoinfo.aaos.org. Mar. 2013 [Online]. Available: http://orthoinfo.aaos.org/topic.cfm?topic=a00412

29. Wolff J. The classic: On the significance of the architecture of the spongy substance for the question of bone growth: a preliminary publication. 1869. Clin Orthop Relat Res. 2011; 469:3077–8. [PubMed: 21866420]

30. Biomechanics of distal radial fractures. [10/8/2015] Aofoundation.org. [Online]. Available: https://www2.aofoundation.org/wps/portal/!ut/p/a0/04_Sj9CPykssy0xPLMnMz0vMAfGjzOKN_A0M3D2DDbz9_UMMDRyDXQ3dw9wMDAzMjfULsh0VAbWjLW0!/?bone=Radius&segment=Distal&showPage=F&contentUrl=srg/popup/further_reading/23/Biomechanics-dist-radFX.jsp

31. Lin W, Ladinsky GA, Wehrli FW, Song HK. Image metric-based (autofocusing) of motiong artifacts in high-resolution trabecular bone imaging. J Magn Reson Imaging. 2007; 26:191–197. [PubMed: 17659555]

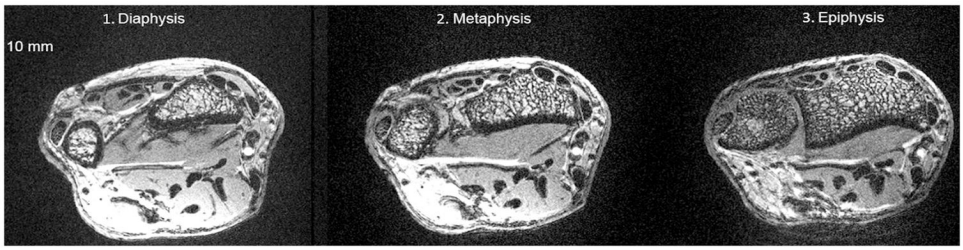

Figure 1.

Axial 7T MR images of the wrist of one subject showing representative images from each site. Note differences in trabeculation pattern at the diaphysis, metaphysis, and epiphysis.

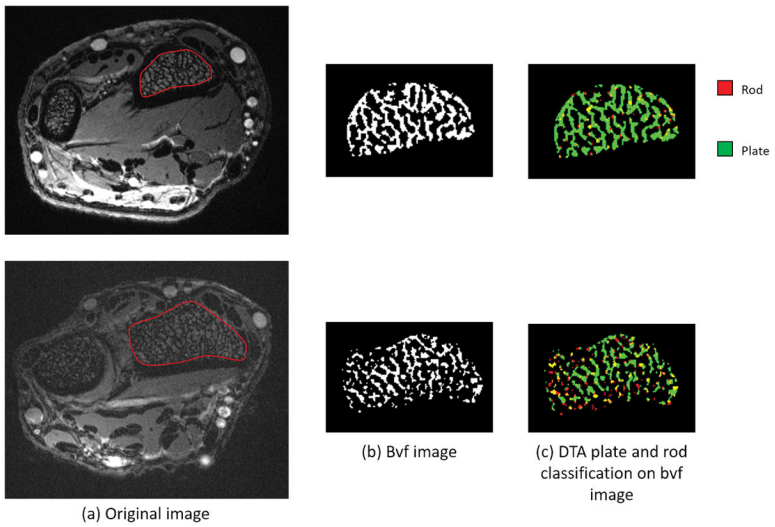

Figure 2.

Axial 7T MR images of the wrist at the epiphysis of two subjects showing representative images of segmentation of trabecular bone, differences in total trabecular bone volume (Bvf image), and differences in microarchitecture as determine by digital tomographic analysis (DTA plate and rod classification on bvf image).

Table 1

Trabecular Total Bone Volume and Microarchitecture Parameters

	Diaphysis	Metaphysis	Epiphysis
Total bone volume (mm^3)	7238±2978 (1825, 12511)	16117±3744 * (7603, 24297)	29383±4765 *† (22961,40929)
Trabecular Number	0.25±0.03 (0.17, 0.30)	0.28±0.02 * (0.25,0.32)	0.29±0.02 * (0.24,0.31)
Trabecular Thickness (μm)	224±16 (200, 263)	225±12 (192, 245)	219±11 (201, 240)
Trabecular Connectivity	0.04±0.01 (0.02, 0.06)	0.05±0.01 * (0.04,0.06)	0.06±0.01 *† (0.04,0.07)
Erosion Index	1.5±0.40 (1.01, 2.42)	1.13±0.30 * (0.85,2.24)	1.24±0.28 *† (0.87, 2.05)

Presented as Mean ± Standard Deviation (Range)

* p <.001 in comparison with diaphysis

† p < .001 in comparison between metaphysis and epiphysis

Table 2

Spearman Correlation of Trabecular Total Bone Volume and Microarchitecture Parameters

	Bone Location	Trabecular Number	Trabecular Thickness	Connectivity	Erosive Index
Total Bone volume	Diaphysis	−.21 (p=.399)	**.77 (p=.000)**	.27 (p=.280)	**−.70 (p=.001)**
	Metaphysis	.19 (p=.396)	**.56 (p=.006)**	.32 (p=.138)	**−.51 (p=.014)**
	Epiphysis	.35 (p=.092)	**.58 (p=.003)**	.31 (p=.138)	**−.65 (p=.001)**
Trabecular Number	Diaphysis		−.33 (p=.176)	**.79 (p=.000)**	−.29 (p=.236)
	Metaphysis		−.13 (p=.553)	**.82 (p=.000)**	**−.59 (p=.003)**
	Epiphysis		.14 (p=.504)	**.78 (p=.000)**	−.34 (p=.101)
Trabecular Thickness	Diaphysis			.02 (p=.938)	**−.67 (p=.002)**
	Metaphysis			−.14 (p=.535)	**−.58 (p=.004)**
	Epiphysis			−.09 (p=.680)	**−.90 (p=.000)**
Connectivity	Diaphysis				**−.54 (p=.020)**
	Metaphysis				−.32 (p=.142)
	Epiphysis				−.10 (p=.628)